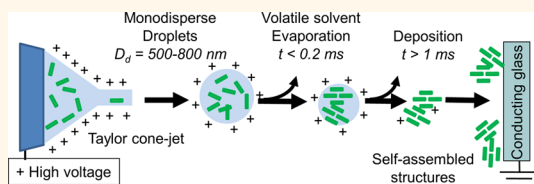


# Aerosolized Droplet Mediated Self-Assembly of Photosynthetic Pigment Analogues and Deposition onto Substrates

Vivek B. Shah and Pratim Biswas\*

Aerosol and Air Quality Research Laboratory, Department of Energy, Environmental and Chemical Engineering, Washington University in St. Louis, St. Louis, Missouri 63130, United States

**ABSTRACT** Self-assembled photosynthetic molecules have a high extinction coefficient and a broad absorption in the infrared region, and these properties can be used to improve the efficiency of solar cells. We have developed a single-step method for the self-assembly of synthetic chlorin molecules (analogues of native bacteriochlorophylls) in aerosolized droplets, containing a single solvent and two solvents, to synthesize biomimetic light-harvesting structures. In the single-solvent approach, assembly is promoted by a concentration-driven process due to evaporation of the solvent. The peak absorbance of Zn(II) 3-(1-hydroxyethyl)-10-phenyl-13<sup>1</sup>-oxophorbine (1) in methanol shifted from 646 nm to 725 nm ( $\sim$ 80 nm shift) after assembly, which is comparable to the shift observed in the naturally occurring assembly of bacteriochlorophyll *c*. Although assembly is thermodynamically favorable, the kinetics of self-assembly play an important role, and this was demonstrated by varying the initial concentration of the pigment monomer. To overcome kinetic limitations, a two-solvent approach using a volatile solvent (tetrahydrofuran) in which the dye is soluble and a less volatile solvent (ethanol) in which the dye is sparingly soluble was demonstrated to be effective. The effect of molecular structure is demonstrated by spraying the sterically hindered Zn(II) 3-(1-hydroxyethyl)-10-mesityl-13<sup>1</sup>-oxophorbine (2), which is an analogue of 1, under similar conditions. The results illustrate a valuable and facile aerosol-based method for the formation of films of supramolecular assemblies.



**KEYWORDS:** supramolecular self-assembly · aerosol route · photosynthetic antenna · bacteriochlorophyll analogues · chlorin

Self-assembled materials are gaining in importance due to their special properties and applications in different areas such as solar cells,<sup>1,2</sup> photonics,<sup>3,4</sup> organic semiconductors,<sup>5,6</sup> recording media,<sup>7</sup> and development of biomaterials.<sup>8,9</sup> Molecular self-assembly is used to synthesize new materials such as liquid crystals<sup>10</sup> and semicrystalline and phase-separated polymers.<sup>11</sup> Molecular self-assembly is defined as spontaneous assembly under equilibrium conditions to form stable aggregates; the process can entail formation of covalent<sup>12</sup> or noncovalent bonds.<sup>13</sup> Traditional synthetic procedures can be utilized to create reasonably large molecules, yet such structures typically lack order on the length scale ( $>10$  nm) desired for many studies. On the other hand, self-assembly is attractive for formation of organized structures or molecular aggregates.<sup>14</sup> Molecular self-assembly takes place due to various

noncovalent interactions such as van der Waals forces, hydrophobic forces, hydrogen bonds, or  $\pi$ -orbital interactions. Molecular self-assembly is not restricted to organic materials but also can encompass inorganic materials such as polyions.<sup>15</sup>

Self-assembled aggregates often exhibit properties distinct from those of individual molecules. Both energy transfer and improved absorption in the near-infrared (NIR) region take place in chlorosomes, wherein bacteriochlorophyll (BChl) *c*, *d*, and *e* molecules are assembled into large architectures. Chlorosomes, the light-harvesting antennas of green sulfur bacteria, serve to absorb light and funnel the resulting energy to a reaction center.<sup>16</sup> Efficient energy transfer takes place when individual molecules are close to each other and oriented for effective coupling of the respective transition dipole moments. The self-assembled aggregates in

\* Address correspondence to pbiswas@wustl.edu.

Received for review October 8, 2013 and accepted January 8, 2014.

Published online January 08, 2014  
10.1021/nn405251h

© 2014 American Chemical Society

the chlorosomes satisfy these conditions for energy transfer. Indeed, green sulfur bacteria survive in low light conditions at 110 m below sea level by capturing and transferring the energy of all incident photons.<sup>17,18</sup> The electronic coupling of BChl *c* molecules to each other also results in a bathochromic shift in peak absorbance from 670 nm, which corresponds to the Q<sub>y</sub> band for monomers, to 749 nm for aggregates. Thus, self-assembled BChl molecules enable chlorosomes to harvest light in the NIR region of the solar spectrum, which contains 26.4% of the total incident solar energy.

These special properties of light absorption and efficient energy transfer make self-assembled structures potentially attractive for applications in photovoltaics.<sup>19</sup> Improved performance was demonstrated when chlorosomes were incorporated in titanium dioxide-based dye-sensitized solar cells.<sup>20</sup> In general, it is tedious to modify the native chlorosomes in size, composition, or other physicochemical attributes, to facilitate detailed experiments. Thus, there is interest in assembling synthetic analogues of the native BChls in an effort to mimic chlorosomes. BChls belongs to a class of molecules that show a characteristic bathochromically shifted absorption for aggregates, called J-aggregates (after the founder Jelley).<sup>21</sup> Among the various J-aggregates, derivatives of porphyrins and chlorins have been extensively studied because of their similarity to BChls and applications for harvesting solar energy. Tailored synthetic analogues also afford an opportunity, in principle, to tune the absorption spectrum to the area of interest in the solar spectrum.

Various chlorins<sup>22–24</sup> and porphyrins<sup>25</sup> have been assembled in solution, and the effects of molecular structure and substituents have been studied extensively. Self-assembled aggregates of chromophores are formed by hydrophobic interactions,<sup>26,27</sup> interaction with nonpolar solvents,<sup>28</sup> evaporating solvent,<sup>19,29</sup> or dispersive halogen interactions.<sup>30</sup> The solution-based assembly of various tetrapyrrole macrocycles has been reviewed by Miyatake and Tamiaki.<sup>31</sup> One of the drawbacks of solution-based methods is the difficulty in controlling the final size of the aggregate. In this regard, the rate of assembly is often faster than the time scale for mixing, making it difficult to control the growth of aggregates.<sup>32</sup> The size of the aggregate determines the spectral properties such as extinction coefficient and wavelength of absorption, which are critical for light harvesting. Hence controlling the size is important for the final application. One approach to control the size of aggregates entails formation as an emulsion using detergents<sup>26</sup> or using amphiphilic molecules.<sup>33</sup> However, in all such methods, transferring the aggregates to a surface is difficult. Since deposition on a surface is essential for numerous fundamental studies as well as device applications,

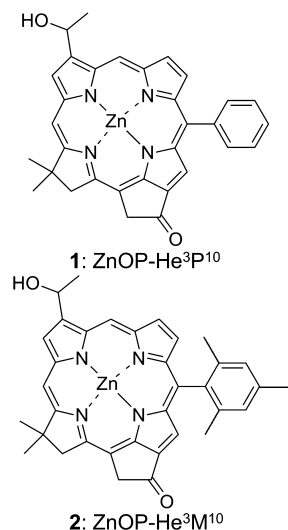


Chart 1. Molecular structure of zinc chlorins (1, 2), with self-assembling properties.

evaporative self-assembly has been used to form self-assembled architectures by spin coating.<sup>19,29</sup> This evaporative technique offers little or no control over the size of aggregates and is typically restricted to use with smooth surfaces. Other approaches rely on formation of Langmuir–Blodgett films<sup>34</sup> when amphiphilic molecules are available, or covalent chemical synthesis with building block chromophores *via* stepwise<sup>35</sup> or polymerization<sup>36</sup> methods.

Aerosol-based methods for synthesis are readily scalable and often entail only a single-step fabrication process. This approach affords a number of advantages over most other methods of assembly. Particles formed after aerosolization can readily be deposited to form thin films. Moreover, using aerosol techniques, the contact of a solvent with the substrate can be avoided, thereby enabling deposition of multiple layers without the risk of washing out preceding layers.<sup>20</sup> The first work to attain nanostructured ordering using aerosols involved the synthesis of mesoporous silica particles by Brinker *et al.*<sup>37</sup> Since then, aerosol-based self-assembly has been widely used to synthesize mesoporous structures.<sup>38–41</sup> Although a wide range of mesoscopic structures have been synthesized by aerosol routes, to our knowledge, supramolecular self-assembly in aerosolized droplets has heretofore not been reported. Some mass spectrometric studies demonstrate evidence of stable molecular aggregates formed by electrospray,<sup>42,43</sup> but such aggregates have not been isolated or characterized by UV–visible absorption spectroscopy. Moreover, in order to use the aerosol technique, detailed understanding of the underlying mechanism of assembly is required.

Here, self-assembly is explored in aerosolized droplets with chlorin molecules **1** and **2** (Chart 1), which are analogues of the natural photosynthetic dye bacteriochlorophyll *c*. Two different approaches, using a

**TABLE 1. Properties of the Spray Solution, Electrospray Conditions for the Spray Solution, and Various Properties of the Sprayed Droplet**

solvent	properties of spray solution				electrospray conditions				properties of sprayed droplets			
	dielectric constant of spray solution	dye concentration range, $\mu\text{M}$	concentration of ammonium acetate, mM	conductivity, $\mu\text{S}/\text{cm}$	flow rate of spray solution	voltage, kV	current, nA	size, $^a$ nm	95% interval for droplet size with $\sigma_g = 1.1, ^b$ nm	average no. of dye molecules per droplet	time of flight, <sup>c</sup> ms	time of evaporation ms
					$\mu\text{L}/\text{min}$							
methanol	33 $\pm$ 0.5	8.8–20.2	5	322 $\pm$ 2	1 $\pm$ 0.01	4.75	260	518 $\pm$ 4	428–626	1190	>1.38	0.043
ethanol–THF (5:4)	15.7 $\pm$ 1.0	13.5–43.9	10	53.4 $\pm$ 0.4	1 $\pm$ 0.01	4.3	130	817 $\pm$ 21	675–988	4650	>1.10	0.115 <sup>d</sup>

<sup>a</sup> Using scaling law equations. <sup>b</sup> Geometric standard deviation for monodisperse droplet.<sup>50</sup> <sup>c</sup> Assuming constant size of the droplet and charge. Actual times will be much larger than the ones estimated for constant size and charge. <sup>d</sup> Using eq 1 and assuming Fuchs correction factor to be 1. For ethanol–THF mixture sequential evaporation of solvents is assumed because THF is highly volatile. The heat transfer effects have been taken into account by using the equation for droplet cooling.<sup>51</sup>

single solvent and two solvents, for molecular self-assembly in aerosolized droplets are examined. The underlying mechanism for assembly, which is different from spray drying, is also elucidated. The applicability of the method to assemble different types of molecules is demonstrated with both the single- and two-solvent approaches.

## RESULTS AND DISCUSSION

On aerosolizing a solution containing the dye molecules, a droplet with a known concentration (or number of monomers) is obtained. As the solvent evaporates, the concentration increases in the droplet, eventually reaching thermodynamically favorable conditions for self-assembly. By controlling the concentration of dye molecules in the solution, the location (or time) in flight at which self-assembly takes place can be varied. The nucleation rate is also an important parameter that determines whether self-assembly takes place before the solvent evaporates. The nucleation rate is a function of dye molecule concentration. The interplay of these various time scales is described in detail in the following sections.

The size of the assembled structures synthesized by the aerosol technique is hard to probe in-flight, because of short time scales ( $\sim 1$  ms) and small size of the self-assembled structures ( $< 50$  nm). Hence the self-assembled structures are characterized after deposition onto a substrate. Since the self-assembled structures are made up of organic molecules, imaging with TEM or characterization by X-ray diffraction does not give insightful results. However, these photosynthetic molecules have a special property that the peak absorption of self-assembled structures shifts because of the excitonic interactions. This set of photosynthetic molecules whose absorption is red-shifted on assembly are called J-aggregates. Hence the self-assembled structures and their size are analyzed by measuring the change in peak absorption by a UV–visible spectrophotometer.

The shift in spectra as a function of size is explained first as it is used to analyze the self-assembly results.

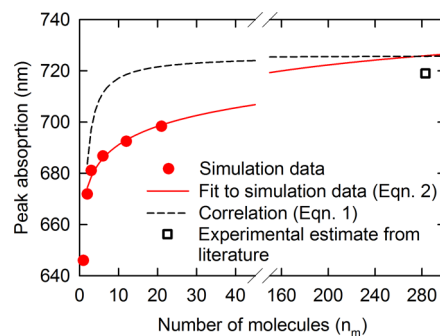


**Figure 1.** Comparison of the simulation data taken from Roden *et al.*<sup>46</sup> to a simplistic correlation (eq 1) for change in peak absorption wavelength with increasing number of molecules present in the self-assembled structure. The experimental estimate is for chlorosomes of *Chloroflexus aurantiacus*, which consist of self-assembled BChl c resulting in a 73 nm shift in spectra.<sup>44</sup>

A single-solvent approach to assemble dye molecules is then discussed. To overcome the kinetic limitations of nucleation over a wider range of initial concentrations of dye molecules and to change the size of the self-assembled structure, a two-solvent approach is then described. The detailed conditions for the experiments are listed in Table 1.

**Shift in Absorption Spectra.** There is a sharp shift in the absorption peak of the self-assembled molecules of J-aggregates in comparison to monomers due to excitonic interactions. It should be noted that a random aggregation that would result in an ordinary spray-drying process will not result in the formation of J-aggregates. For these self-assembled structures, as the number of dye molecules increases, the peak absorption is more red-shifted as shown in Figure 1. However when a large number of molecules are present, the shift gets saturated. The shift due to a large number of self-assembled molecules is commonly observed in J-aggregates. However there is limited experimental data for correlating size with a shift in peak absorption.<sup>44</sup> For a linear one-dimensional self-assembled aggregate with circular boundary conditions, the energy of electronic transition and the

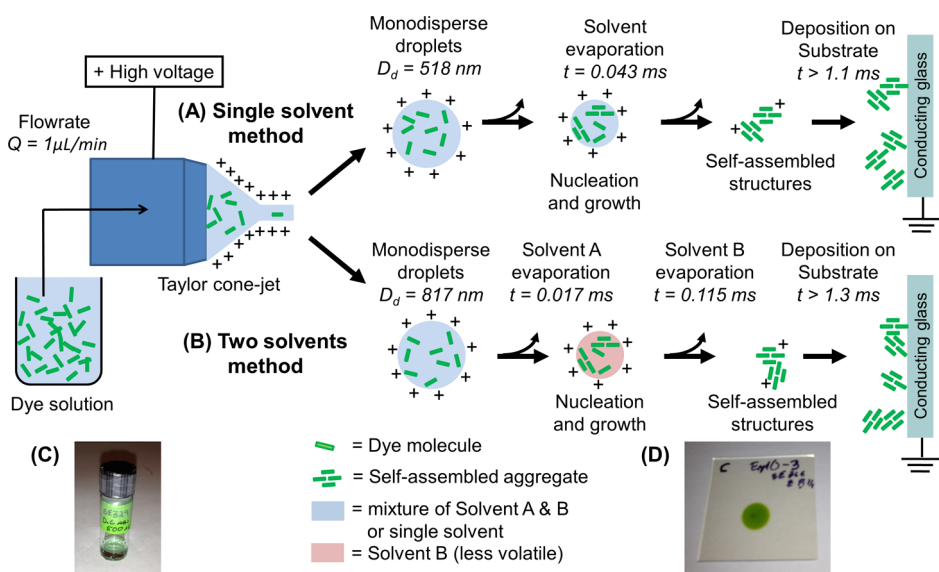


**Figure 2.** Schematic of the electrospray deposition system and proposed mechanisms for self-assembly of chlorin molecules in a droplet by (a) the single-solvent and (b) the two-solvent method in which solvent A is more volatile than solvent B. (c) Image of a spray solution of 1 prepared by dissolution in ethanol-THF. (d) Image of a conducting glass substrate after electrospray deposition of 1.

physical size are related:<sup>45</sup>

$$\begin{aligned} E_{n_m} &= E_{\infty} - (E_{\infty} - E_1)/n_m \\ \because E &= hc/\lambda \quad (1) \\ 1/\lambda_{n_m} &= 1/\lambda_{\infty} - (1/\lambda_{\infty} - 1/\lambda_{n_m})/n_m \end{aligned}$$

where  $E_{n_m}$  is the transition energy of an aggregate consisting of  $n_m$  number of molecules,  $E_1$  is the transition energy of an isolated molecule, and  $E_{\infty}$  is the transition energy of an infinite chain. The transition energy can be converted to peak absorption wavelength ( $\lambda$ ) as a function of number of molecules and is shown in Figure 1. This equation is compared to simulation of absorption spectra by Roden *et al.*<sup>46</sup> for linear chains of molecules with a  $-0.15$  eV interaction potential at 0 K. Since the correlation fails to capture the shift at a fewer number of molecules, the simulation data are used for analysis. The simulation data by Roden *et al.*<sup>46</sup> are fitted with an equation to aid analysis when a large number of molecules are present in a self-assembled structure. The resulting equation for  $n_m \geq 2$  is

$$\lambda_p = 10.41 \ln(n_m) + 667.15 \quad (2)$$

where  $n_m$  is the number of molecules and  $\lambda_p$  is the peak absorption wavelength in nm. As shown in the figure, the correlation overestimates the shift compared to simulation. The shift in absorption given by eq 2 may be oversimplistic; however due to lack of knowledge of the self-assembled structure of **1** or **2**, it is used to explain the results under the assumption that peak shifts remain the same at 293 K, the temperature at which measurements are made.

For these molecules the shift is dependent on the interaction distance, orientation, and dipole strength. A protein network or external factors would be required to force the interaction of dyes in different orientations apart from the thermodynamically favorable structures. Since there are no external factors, only one thermodynamically favorable structure is assumed to be formed using techniques described in this work.

**Single-Solvent Method.** In the single-solvent method, a dye is dissolved in methanol (solvent) and the solution is then atomized by electrospray. An electrospray atomization methodology is used because monodisperse droplets of small sizes are readily produced. Furthermore, the droplets are charged and the charge is transferred to the self-assembled structures. These charged assembled structures are then readily deposited onto the substrate or desired surface using the electric field. After atomization, the solvent evaporates and the droplet is supersaturated with the dye molecules. This promotes nucleation into self-assembled structures as shown in Figure 2a. However there are certain conditions (lower initial concentrations) where the dye molecules do not assemble due to kinetic reasons. In order to study the kinetics in detail, the initial concentration of **1** in the spray solution was varied from  $8.8 \mu\text{M}$  to  $20.2 \mu\text{M}$ . The kinetics of self-assembly is analyzed by comparing the time constants for evaporation and nucleation and the time available for nucleation. The time available for nucleation is the time to complete solvent evaporation after the droplet attains a critical saturation ratio.<sup>47,48</sup>

Using the scaling laws for electrospray,<sup>47,48</sup> the diameter of the droplet is estimated to be 518 nm. The size of the droplets decreases with time due to

evaporation of the solvent. The time taken for complete evaporation of solvent ( $\tau_e$ ) is

$$\tau_e = \frac{R\rho_d d_i^2 T_d}{8D_v M p_d} \propto d_i^2 \quad (3)$$

where  $R$  is the universal gas constant,  $\rho_d$  is the density of the solvent,  $d_i$  is the initial droplet diameter,  $T_d$  is the temperature of the droplet,  $D_v$  is the diffusion coefficient of the vapor,  $M$  is the molecular weight, and  $p_d$  is the partial pressure of the solvent vapors. Using this equation, the estimated time for evaporation of a methanol droplet of diameter 518 nm is 43  $\mu$ s. The estimated time for the droplet to reach the substrate at a distance of 10 mm due to electrostatic force without evaporation is >1.3 ms. Hence the selected distance between the electrospray capillary needle and substrate ensures complete evaporation of the solvent before the dyes are deposited onto the substrate. Thus, the thermodynamic criterion of supersaturation is reached for all our selected experimental conditions (as the droplet evaporation time is much smaller than the transit time to the deposition substrate).

As the droplet shrinks in size due to evaporation, the concentration of the dye inside the droplet ( $c$ ) increases with time. Beyond the equilibrium concentration ( $c_e$ ), the solution gets supersaturated. The relation between the saturation ratio and droplet size is given as

$$S = \frac{c}{c_e} = \frac{c_i d_i^3}{c_e d^3} \quad (4)$$

where  $c_i$  is the initial concentration,  $d_i$  is the initial diameter of the droplet, and  $d$  is the droplet diameter at time  $t$ . The size of the evaporating droplet at any time using eq 3 is given as

$$d(t)/d_i = (1 - t/\tau_e)^{1/2} \quad (5)$$

Using this expression, the saturation ratio inside the droplet as a function of time is given by

$$S = \frac{c_i}{c_e(1 - t/\tau_e)^{3/2}} \quad (6)$$

Figure 3a shows the variation of saturation ratio with time for different initial concentrations. Higher initial concentrations result in higher saturation ratios at any given time. As the solvent evaporates, resulting high saturation ratios promote nucleation of the dye molecules and separation of phases. The change in free energy for phase separation is given by

$$\Delta G = 4\pi r^2 \gamma + \frac{4}{3} \pi r^3 \Delta g_v \quad (7)$$

where  $\gamma$  is the surface energy,  $r$  is the radius of the assembled nuclei, and  $\Delta g_v$  is the difference in free energy in assembled phase from monomers in solution.  $\Delta g_v$  is a function of saturation ratio ( $S$ ) and is given by

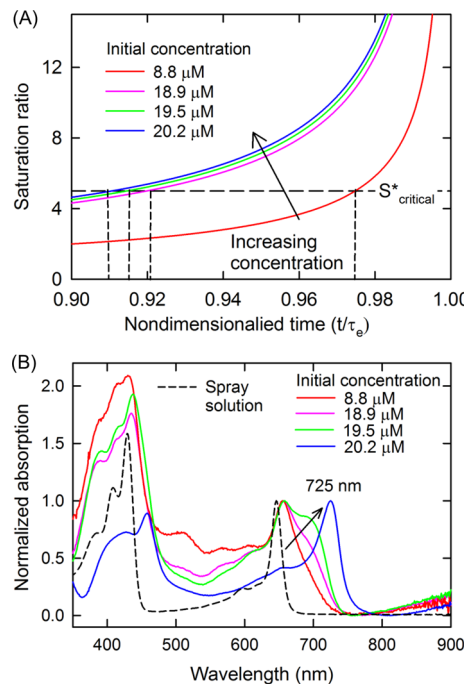


**Figure 3.** (a) Change in saturation ratio inside the evaporating droplet as a function of nondimensionalized time. (b) Comparison of the normalized UV-vis absorption spectrum after deposition at various initial concentration of 1 in spray solution (colored solid lines) to its spray solution in methanol (black broken line).

$$\Delta g_v = -\frac{kT \ln S}{\Omega} \quad (8)$$

where  $k$  is the Boltzmann constant,  $T$  is the temperature, and  $\Omega$  is the molecular volume. When the saturation ratio is greater than 1,  $\Delta g_v$  is negative. At a saturation ratio ( $S$ ) greater than the critical saturation ratio ( $S^*$ ), the change in free energy will be negative and hence the nucleation into self-assembled structures will be favored. The critical saturation ratio ( $S^*$ ) is the value of  $S$  when the nucleation rate is greater than 1 nucleation/second inside the droplet. Thus irrespective of the initial concentration, thermodynamically, nucleation is expected to take place inside the droplets once the critical saturation ratio is exceeded. However this is contrary to some of the experimental observations. Figure 3b shows the effect of initial concentration on the absorption spectra of the deposited aggregates. The shift in peak absorption and the spectra varies with the initial concentration, which means that assembly does not take place for all the cases. In order to understand the reasons, the kinetics of nucleation of self-assembled structures are analyzed.

The nucleation into a self-assembled structure takes finite time after the critical saturation ratio is reached; that is, there is a delay before nucleation takes place. The delay time for nucleation ( $\tau_d$ ) is given by the following equation:<sup>49</sup>

$$\tau_d = \frac{32}{\pi^2} \frac{v_0 \sigma^2}{\gamma^* (kT)^2 D N c_e S (\ln S)^3} \quad (9)$$

**TABLE 2. Values of the Constants for 1 for Estimating the Time Delay for Nucleation**

constant	value
molecular volume ( $v_0$ )	$0.5 \times 10^{-27} \text{ m}^3$
surface energy ( $\sigma$ )	$0.03 \text{ J/m}^2$
diffusion coefficient ( $D$ )	$1.00 \times 10^{-9} \text{ m}^2/\text{s}$
equilibrium solubility ( $c_e$ )	$30 \mu\text{M}$
saturation ratio ( $S$ )	40
temperature <sup>a</sup> ( $T$ )	268 K
delay time ( $\tau_d$ )	$35.9 \mu\text{s}$

<sup>a</sup> Steady-state temperature for an evaporating droplet of methanol with diameter 518 nm.

where  $v_0$  is the molecular volume of dye,  $\sigma$  is the surface energy of the self-assembled material,  $\gamma^*$  is the accommodation coefficient in solution, which is  $\sim 1$ ,  $k$  is the Boltzmann constant,  $T$  is the temperature,  $D$  is the monomer diffusion coefficient in the solvent, solvent,  $N$  is Avogadro number,  $c_e$  is the equilibrium solubility, and  $S$  is the saturation ratio. At a critical saturation ratio ( $S^*$ ), the time delay for nucleation will be constant irrespective of the initial concentration. Assuming the values of parameters listed in Table 2 for **1**, the delay is estimated to be  $35.9 \mu\text{s}$ . The estimated time delay is on the order of evaporation time of solvent.  $t_d$  can be normalized by the evaporation time for the droplet to give a delay time constant

$$\tau_d = t_d/\tau_e \quad (10)$$

The dimensionless time available when  $S$  is greater than  $S^*$  before the solvent completely evaporates is

$$\tau_a = t_a/\tau_e = 1 - t^*/\tau_e \quad (11)$$

where  $t^*$  is the time at which the droplet reaches  $S^*$ . Thus for assembly to take place, the delay time for nucleation should be less than the time available before the solvent from the droplet completely evaporates, *i.e.*,  $\tau_d < \tau_a$ . If the time available is less than the delay time for nucleation, the dyes will nucleate into clusters smaller than stable nuclei or result in random aggregation.

Since the exact value of  $c_e$  and other constants is not known, Figure 3a shows the qualitative relation between the delay in nucleation time and the time available for nucleation depending on the initial concentration. Figure 3b shows the experimental results for assembly with the change in initial concentration. The molecules at low concentration, corresponding to  $8.8 \mu\text{M}$ , result in a 10 nm shift in the absorption peak, which indicates the formation of unstructured (amorphous-like) aggregates without any long-range order. Since at low concentration there is insignificant time for nucleation, random aggregation of the dye molecules takes place as evaporation proceeds to completion. This random agglomeration is similar to an uncontrolled spray-drying process. On increasing

the monomer concentration to 18.9 and  $19.5 \mu\text{M}$ , the dyes give rise to intermediate size clusters, resulting in a shoulder at 690–710 nm. The dyes at these concentrations reach the critical saturation ratio and form clusters. However due to solvent evaporation, their growth into stable nuclei is incomplete. On increasing the concentration to  $20.2 \mu\text{M}$ , self-assembled structures give rise to a sharp, bathochromically shifted peak at 725 nm. As shown in the figure, in this case there is enough time for the monomers to nucleate into self-assembled structures since  $\tau_a > \tau_d$ . Thus to form self-assembled structures using single-solvent assembly, the solvent should be selected such that  $\tau_a > \tau_d$ . Using a single-solvent method, the saturation ratio cannot be changed independently of the droplet size (refer to eq 4). Moreover, in the single-solvent method the maximum concentration is limited by the solubility of the dye in the solvent. Hence for some molecules that require very high saturation ratio to assemble, the condition of  $\tau_d < \tau_a$  may not be satisfied for certain droplet sizes.

**Two-Solvent Method.** A two-solvent combination is used to overcome the kinetic limitations and the dependence of saturation ratio on the droplet size for a single solvent. In the two-solvent method, solvent A that easily dissolves the dye molecules is selected such that it is more volatile than solvent B, in which the dye is sparingly soluble. Figure 2b shows the proposed mechanism for self-assembly with the two solvents. Tetrahydrofuran (THF), which dissolves the dye, is selected as solvent A and ethanol (Et), in which the dye is sparingly soluble, is selected as solvent B. THF being volatile evaporates first, supersaturating the ethanol droplets with the dye molecules. In this case, the solution is supersaturated due to evaporation of volatile solvent (THF). Hence the saturation ratio is dependent on the solvent composition and not on the droplet size. After the ethanol solution is supersaturated, the dye molecules nucleate into self-assembled structures. Over time ethanol completely evaporates and the charged aggregate of the dye is deposited on the substrate due to electrostatic force.

In the single-solvent method, the dye is selected such that it is sparingly soluble, so that it will nucleate at high saturation ratio. In contrast, in the two-solvent method the solvent in which the dye is highly soluble is mixed with the solvent in which the dye is sparingly soluble. Thus a higher initial concentration of dye in the spray solution can be attained, which is not possible with the single-solvent method. A high initial concentration translates to a higher saturation ratio in the sprayed droplet after evaporation of the volatile solvent A (THF). The longer time available for nucleation due to lower volatility of ethanol and higher saturation ratio, which ensures shorter delay time for nucleation, both help satisfy the condition  $\tau_a > \tau_d$ . Thus on using a two-solvent method, the kinetic limitations to the

assembly process are eliminated. Since there are no kinetic limitations and saturation ratio can be independently controlled, the size of the self-assembled structure could be altered to change the absorbance spectra. In order to study the size dependence with supersaturation, experiments at different initial concentration from 13.5 to 43.9  $\mu\text{M}$  in ethanol–tetrahydrofuran (Et–THF) were conducted. The results for the size dependence of concentration were analyzed by the classical nucleation theory.

Monodispersed droplets of 817 nm diameter are electrosprayed. After the droplet is sprayed the solvents start evaporating. The estimated time for evaporation of ethanol–THF droplets of 817 nm diameter is 115  $\mu\text{s}$ . The time for evaporation is much shorter than >1.1 ms taken to traverse the distance between needle and substrate without solvent evaporation. Thus the solvents evaporate before deposition. The volatile solvent THF evaporates first, supersaturating the ethanol solution. The saturation ratio can be expressed as

$$S = \frac{mc_i}{c_e} \quad (12)$$

where  $m$  is the enhancement in concentration due to evaporation of solvent,  $c_i$  is the initial concentration, and  $c_e$  is the equilibrium concentration. The dye molecules nucleate, after the saturation ratio crosses the critical value. Since there are two solvents, the solvent with lower volatility ensures sufficient time for nucleation and the nucleation is not limited by kinetics. The size of nuclei ( $d_p^*$ ) by classical nucleation theory is given as

$$d_p^* = \frac{4\sigma v_m}{kT \ln S} \quad (13)$$

where  $\sigma$  is the surface energy,  $v_m$  is the molecular volume, and  $S$  is the saturation ratio. Thus the number of molecules ( $n_m$ ) in the nuclei is given by

$$n_m = \frac{\pi}{6} \left( \frac{4\sigma v_m^{2/3}}{kT \ln S} \right)^3 \quad (14)$$

On varying the initial concentration in the spray solution, different saturation ratios can be attained. Substituting eq 12 in eq 14 gives the relation between number of molecules in the self-assembled structure and the initial concentration:

$$n_m = \frac{k_1}{(\ln c_i - \ln k_2)^3} \quad (15)$$

where  $k_1 = (\pi/6)[4\sigma v_m^{2/3}/kT]^3$  and  $k_2 = c_e/m$  are the new constants.

Figure 4a shows the shift in absorption spectra at various initial concentrations from 13.5 to 43.9  $\mu\text{M}$  on the self-assembly of **1**. The peak shift for these concentrations and the number of molecules present in the self-assembled structure estimated using eq 2 are both summarized in Table 3. At the higher

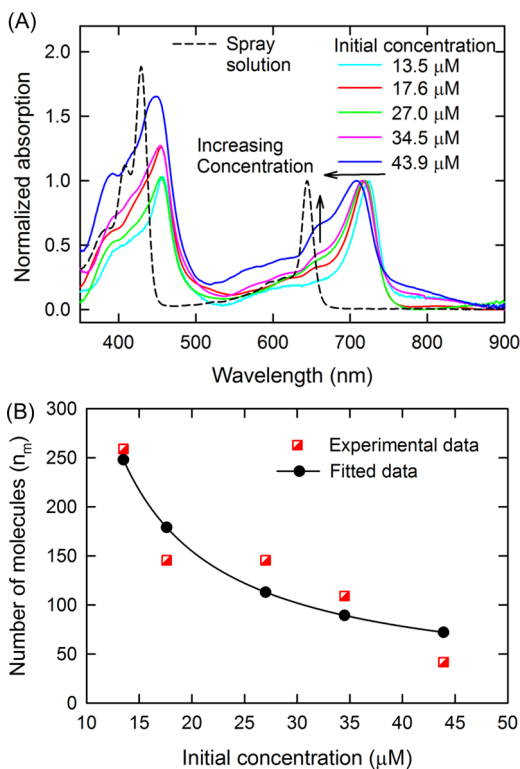


**Figure 4.** (a) Comparison of the normalized UV–vis absorption spectrum after deposition at various monomer concentrations of **1** in spray solution (colored solid lines) compared to spray solution in ethanol–THF (black broken line). (b) Data for shift in absorption due to different initial concentrations summarized in Table 3 and the fitted curve after optimizing constants in eq 15.

**TABLE 3. Experimental Results Using the Two-Solvent Method for the Self-assembly of **1****

initial concentration ( $c_i$ ), $\mu\text{M}$	peak wavelength, nm	shift in absorption <sup>a</sup> ( $\Delta\lambda$ ), nm	no. of molecules ( $n_m$ ) <sup>b</sup>
13.5	725	81	259
17.6	719	75	145
27	719	75	145
34.5	716	72	109
43.9	706	62	41

<sup>a</sup> Calculated for peak monomer absorption of **1** as 644 nm. <sup>b</sup> Calculated using the fitting eq 2 plotted in Figure 1

concentrations, the peak corresponding to the aggregate is less red-shifted, and at lower concentrations the aggregate peak is more red-shifted (bathochromically shifted). In order to establish a quantitative relationship between initial concentration and the number of molecules, eq 15 is a fit to the experimental data listed in Table 3. Since the saturation ratio has to be greater than 1,  $k_2$  should be less than the minimum initial concentration (<13.5  $\mu\text{M}$ ). The parameters  $k_1$  and  $k_2$  from eq 15 are fitted using the *nlinfit* function in MATLAB to the number of molecules and the initial concentration data in Table 3. As shown in Figure 4b, a good fit to the experimental data is obtained.

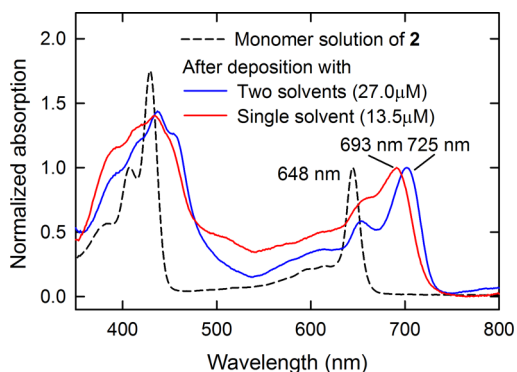


Figure 5. Self-assembly results using **2**, which is analogous to **1**, using the single-solvent and two-solvent methods.

The values obtained from fitting correspond to  $k_1 = 3079 \pm 2643$  and  $k_2 = 1.33 \pm 0.95$ . Using  $k_1 = 3079$  and assuming the molecular volume to be  $\sim 0.5 \text{ nm}^3$ , the estimated value of surface energy is  $0.027 \text{ N/m}$ . The surface energy is less than the values for the organic molecules reported in the literature, which is in the range  $0.08\text{--}0.16 \text{ N/m}$ . Lower than literature values for surface energy could be because the reported values are with respect to vacuum; however the molecules of **1** are in contact with ethanol. The other reason for the lower estimate for surface energy could be due to heterogeneous nucleation at the air–liquid interface. Using  $k_2$  the saturation ratios are estimated to be in range of 10.1 to 32.9, for the concentrations used in this study. The variation between the fitted data and the experimental data is due to possible differences in the shape of self-assembled structures or the simulated spectra. The number of molecules in each aggregate (Table 1) is less than the total dye molecules in each droplet (Table 3), thus implying that there are multiple centers of nucleation. This also clearly illustrates that the self-assembly is different from purely spray drying, which does not require any thermodynamic driving force and results in randomly oriented molecules.

Figure 5 shows the spectra of the deposits of **2**, sprayed at  $13.5 \mu\text{M}$  concentration using methanol as solvent and  $27.0 \mu\text{M}$  concentration using ethanol–THF as solvents. This molecule has similar characteristics to

that of **1**, except for the substituent group. The shifts observed correspond to 693 nm for the single-solvent method and 725 nm for the two-solvent method, as shown in Figure 5. Clearly, both methods can be used to assemble **2**. Thus the aerosol-based molecular assembly technique can be used for other self-assembling molecules.

## CONCLUSIONS

Supramolecular assembly in an aerosolized droplet has been demonstrated for the first time in this work. Self-assembly that resulted in formation of J-aggregates was successfully promoted due to the strict control of droplet size using an electrohydroatomization process. By self-assembling bacteriochlorophyll *c* analogues, synthetic mimics of light-harvesting antennas were synthesized and also deposited as films. This aerosol-based method is a novel technique to synthesize and deposit self-assembled structures in one step. Using the aerosol technique, higher control over deposition and the size of the self-assembled structures can be exercised, in contrast to a simple spray-drying process. In the single solvent method, although assembly is thermodynamically favored, kinetics of nucleation are important for eventual assembly. These kinetic limitations on the time available for assembly due to evaporation of the droplet in the single-solvent method can be overcome by using two solvents. On using two solvents, further control over the size of nuclei of the self-assembled structure was demonstrated. Similar control using solution-based methods has not been possible because of difficulties in controlling nucleation, which takes place on short time scales. The study of these two cases (single-solvent and two-solvent methods) suffices to explain most of the practical solvent combinations and their effects on the mechanism of assembly. The self-assembled structures, especially of porphyrin derivatives, can be used for a wide range of applications such as light harvesting in up-conversion systems, solar cells, and/or for synthesizing metal organic frameworks. A wide range of molecules so far assembled using solution techniques could be assembled and deposited with greater control using the aerosol technique.

## METHODS

**Spray Solution Composition and Characterization.** The molecular structures of the dyes used in this work are shown in Chart 1. The dyes have a keto group, a hydroxyl group, and a metal center, which are required for self-assembly.<sup>22</sup> The dye molecules were dissolved in either methanol or a mixture of ethanol and tetrahydrofuran (Et–THF). Anhydrous ethanol (200 proof from Sigma-Aldrich, St. Louis, MO, USA), THF (inhibitor free, CromaSolv Plus, Sigma-Aldrich), and methanol (CromaSolv, Sigma-Aldrich) were used for the experiments. On dissolution in either methanol or Et–THF solvent, these dyes show a characteristic  $Q_y$  absorption at 646 nm for **1** and 648 nm for **2**. The UV–visible

absorption of the spray solution and the deposits is measured on a UV–visible spectrophotometer (Cary 100, Agilent Technologies, Santa Clara, CA, USA). The absorbance of the dye molecules in solution at the  $Q_y$  band is converted to concentration using the extinction coefficient ( $\epsilon = 74 \text{ mM}^{-1} \text{ cm}^{-1}$ ) of the natural dye bacteriochlorophyll *c*. The dissolved dye molecules are present as monomers in the solution before spraying, as evidenced by the absence of an aggregate peak in the absorption spectrum. Ammonium acetate is added to make the solution conducting for electrospray atomization, and it also acts as a buffer. Conductivity of the spray solution is measured using a digital conductivity meter (Dip Cell, Pt plate surface,

model 1054, Amber Science Inc., OR, USA). Since methanol is highly conducting, a lower ammonium acetate concentration of 5 mM is employed for methanol compared to 10 mM for ethanol–THF.

**Electrospray Atomization.** Figure 2 shows the schematic of a laboratory electrospray setup for synthesizing and depositing the self-assembled structures. The spray solution is pumped through a tapered needle with an inner diameter of 125  $\mu$ m attached to a syringe. High voltage (4–4.5 kV) is applied between the needle and a grounded substrate to form a cone jet. The spray is delivered onto a substrate, transparent conducting fluorine-doped tin oxide (FTO), placed at a distance of 10 mm from the tip of the needle. The cone jet is visually monitored using a digital optical microscope (QX5, Digital Blue, Atlanta, GA, USA). The current is monitored with an ammeter (6485 Picoammeter, Keithley, Cleveland, OH, USA) to ensure operation in cone jet mode. The scaling law equations are used to calculate the size of a droplet sprayed based on the solution flow rate, conductivity, and dielectric constant.<sup>47,50</sup> Ammonium acetate decomposes and escapes into the surrounding air before deposition of the dye molecules. Thus ammonium acetate does not hamper assembly.

**Characterization of the Deposit.** The self-assembled structures are deposited on glass slides coated with FTO to improve conductivity. After deposition, the slides are immediately characterized for the UV–vis absorption spectra.

**Conflict of Interest:** The authors declare no competing financial interest.

**Acknowledgment.** This work was supported by the Photoprotective Antenna Research Center (PARC), an Energy Frontier Research Center funded by the U.S. Department of Energy, Office of Science, Office of Basic Energy Sciences, under Award Number DE-SC0001035. V.S. thanks McDonnell International Scholars Academy for the fellowship to pursue a Ph.D. at Washington University in St. Louis. The authors thank Prof. Dewey Holten for stimulating discussions and Joseph Springer for help with spectroscopy and sample preparations. The authors also thank Prof. Jonathan Lindsey and Olga Mass, from North Carolina State University, for providing the *de novo* synthesized dye molecules.

## REFERENCES AND NOTES

- Peet, J.; Heeger, A. J.; Bazan, G. C. "Plastic" Solar Cells: Self-Assembly of Bulk Heterojunction Nanomaterials by Spontaneous Phase Separation. *Acc. Chem. Res.* **2009**, *42*, 1700–1708.
- Tange, R.; Inai, K.; Sagawa, T.; Yoshikawa, S. Application of Self-Assembling Photosynthetic Dye for Organic Photovoltaics. *J. Mater. Res.* **2011**, *26*, 306–310.
- Fiorini, C.; Charra, F. Self-Assembly: Mastering Photonic Processes at Nanoscale. *Opto-Electron. Rev.* **2010**, *18*, 376–383.
- Tam, J. M.; Tam, J. O.; Murthy, A.; Ingram, D. R.; Ma, L. L.; Travis, K.; Johnston, K. P.; Sokolov, K. V. Controlled Assembly of Biodegradable Plasmonic Nanoclusters for near-Infrared Imaging and Therapeutic Applications. *ACS Nano* **2010**, *4*, 2178–2184.
- Kim, D. H.; Lee, D. Y.; Lee, H. S.; Lee, W. H.; Kim, Y. H.; Han, J. I.; Cho, K. High-Mobility Organic Transistors Based on Single-Crystalline Microribbons of Triisopropylsilylithiyl Pentacene *via* Solution-Phase Self-Assembly. *Adv. Mater.* **2007**, *19*, 678–682.
- Palmer, R. E.; Robinson, A. P. G.; Guo, Q. How Nanoscience Translates into Technology: The Case of Self-Assembled Monolayers, Electron-Beam Writing, and Carbon Nanomembranes. *ACS Nano* **2013**, *7*, 6416–6421.
- Lee, C.; Metteer, J.; Narayanan, V.; Kan, E. Self-Assembly of Metal Nanocrystals on Ultrathin Oxide for Nonvolatile Memory Applications. *J. Electron. Mater.* **2005**, *34*, 1–11.
- Zhang, S. Fabrication of Novel Biomaterials through Molecular Self-Assembly. *Nat. Biotechnol.* **2003**, *21*, 1171–1178.
- Hirose, T.; Maeno, Y.; Hidema, Y. Photocatalytic Carbon Dioxide Photoreduction by  $\text{Co}(\text{Bpy})_3^{2+}$  Sensitized by  $\text{Ru}(\text{Bpy})_3^{2+}$  Fixed to Cation Exchange Polymer. *J. Mol. Catal. A: Chem.* **2003**, *193*, 27–32.
- Schmidt-Mende, L.; Fechtenkotter, A.; Mullen, K.; Moons, E.; Friend, R. H.; MacKenzie, J. D. Self-Organized Discotic Liquid Crystals for High-Efficiency Organic Photovoltaics. *Science* **2001**, *293*, 1119–1122.
- De Rosa, C.; Park, C.; Thomas, E. L.; Lotz, B. Microdomain Patterns from Directional Eutectic Solidification and Epitaxy. *Nature* **2000**, *405*, 433–437.
- Lindsey, J. S. Self-Assembly in Synthetic Routes to Molecular Devices. Biological Principles and Chemical Perspectives: A Review. *New J. Chem.* **1991**, *15*, 153–180.
- Whitesides, G. M.; Mathias, J. P.; Seto, C. T. Molecular Self-Assembly and Nanochemistry – a Chemical Strategy for the Synthesis of Nanostructures. *Science* **1991**, *254*, 1312–1319.
- Whitesides, G. M.; Grzybowski, B. Self-Assembly at All Scales. *Science* **2002**, *295*, 2418–2421.
- Miras, H. N.; Wilson, E. F.; Cronin, L. Unravelling the Complexities of Inorganic and Supramolecular Self-Assembly in Solution with Electrospray and Cryospray Mass Spectrometry. *Chem. Commun.* **2009**, 1297–1311.
- Frigaard, N.-U.; Bryant, D. Chlorosomes: Antenna Organelles in Photosynthetic Green Bacteria. In *Complex Intracellular Structures in Prokaryotes*; Shively, J., Ed.; Springer: Berlin, 2006; Vol. 2, pp 79–114.
- Overmann, J.; Cypionka, H.; Pfennig, N. An Extremely Low-Light-Adapted Phototrophic Sulfur Bacterium from the Black-Sea. *Limnol. Oceanogr.* **1992**, *37*, 150–155.
- Blankenship, R. E. *Molecular Mechanisms of Photosynthesis*; Blackwell Science: Oxford, 2002.
- Huijser, A.; Marek, P. L.; Savenije, T. J.; Siebbeles, L. D. A.; Scherer, T.; Hauschild, R.; Szmytkowski, J. d.; Kalt, H.; Hahn, H.; Balaban, T. S. Photosensitization of  $\text{TiO}_2$  and  $\text{SnO}_2$  by Artificial Self-Assembling Mimics of the Natural Chlorosomal Bacteriochlorophylls. *J. Phys. Chem. C* **2007**, *111*, 11726–11733.
- Modesto-Lopez, L. B.; Thirsmen, E. J.; Collins, A. M.; Blankenship, R. E.; Biswas, P. Electrospray-Assisted Characterization and Deposition of Chlorosomes to Fabricate a Biomimetic Light-Harvesting Device. *Energy Environ. Sci.* **2010**, *3*, 216–222.
- Jelley, E. E. Spectral Absorption and Fluorescence of Dyes in the Molecular State. *Nature* **1936**, *138*, 1009–1010.
- Mass, O.; Pandithavida, D. R.; Ptaszek, M.; Santiago, K.; Springer, J. W.; Jiao, J.; Tang, Q.; Kirmaier, C.; Bocian, D. F.; Holten, D.; Lindsey, J. S. De Novo Synthesis and Properties of Analogs of the Self-Assembling Chlorosomal Bacteriochlorophylls. *New J. Chem.* **2011**, *35*, 2671–2690.
- Huber, V.; Katterle, M.; Lysetska, M.; Würthner, F. Reversible Self-Organization of Semisynthetic Zinc Chlorins into Well-Defined Rod Antennae. *Angew. Chem., Int. Ed.* **2005**, *44*, 3147–3151.
- Roger, C.; Muller, M. G.; Lysetska, M.; Miloslavina, Y.; Holzwarth, A. R.; Würthner, F. Efficient Energy Transfer from Peripheral Chromophores to the Self-Assembled Zinc Chlorin Rod Antenna: A Bioinspired Light-Harvesting System to Bridge the "Green Gap". *J. Am. Chem. Soc.* **2006**, *128*, 6542–6543.
- Balaban, T. S. Tailoring Porphyrins and Chlorins for Self-Assembly in Biomimetic Artificial Antenna Systems. *Acc. Chem. Res.* **2005**, *38*, 612–623.
- Miyatake, T.; Tamiaki, H.; Holzwarth, A. R.; Schaffner, K. Self-Assembly of Synthetic Zinc Chlorins in Aqueous Microheterogeneous Media to an Artificial Supramolecular Light-Harvesting Device. *Helv. Chim. Acta* **1999**, *82*, 797–810.
- Shahar, C.; Baram, J.; Tidhar, Y.; Weissman, H.; Cohen, S. R.; Pinkas, I.; Rybtchinski, B. Self-Assembly of Light-Harvesting Crystalline Nanosheets in Aqueous Media. *ACS Nano* **2013**, *7*, 3547–356.
- Miyatake, T.; Tamiaki, H.; Holzwarth, A. R.; Schaffner, K. Artificial Light-Harvesting Antennae: Singlet Excitation Energy Transfer from Zinc Chlorin Aggregate to Bacteriochlorin in Homogeneous Hexane Solution. *Photochem. Photobiol.* **1999**, *69*, 448–456.

29. Misawa, K.; Ono, H.; Minoshima, K.; Kobayashi, T. New Fabrication Method for Highly Oriented J-Aggregates Dispersed in Polymer-Films. *Appl. Phys. Lett.* **1993**, *63*, 577–579.

30. Mayerhoffer, U.; Wurthner, F. Halogen-Arene Interactions Assist in Self-Assembly of Dyes. *Angew. Chem., Int. Ed.* **2012**, *51*, 5615–5619.

31. Miyatake, T.; Tamiaki, H. Self-Aggregates of Natural Chlorophylls and Their Synthetic Analogues in Aqueous Media for Making Light-Harvesting Systems. *Coord. Chem. Rev.* **2010**, *254*, 2593–2602.

32. Horn, D.; Rieger, J. Organic Nanoparticles in the Aqueous Phase - Theory, Experiment, and Use. *Angew. Chem., Int. Ed.* **2001**, *40*, 4330–4361.

33. Numata, M.; Kinoshita, D.; Taniguchi, N.; Tamiaki, H.; Ohta, A. Self-Assembly of Amphiphilic Molecules in Droplet Compartments: An Approach toward Discrete Submicrometer-Sized One-Dimensional Structures. *Angew. Chem., Int. Ed.* **2012**, *51*, 1844–1848.

34. Mobius, D.; Kuhn, H. Energy-Transfer in Monolayers with Cyanine Dye Sheibe Aggregates. *J. Appl. Phys.* **1988**, *64*, 5138–5141.

35. Jiao, J.; Anariba, F.; Tiznado, H.; Schmidt, I.; Lindsey, J. S.; Zaera, F.; Bocian, D. F. Stepwise Formation and Characterization of Covalently Linked Multiporphyrin-Imide Architectures on Si(100). *J. Am. Chem. Soc.* **2006**, *128*, 6965–6974.

36. Liu, Z.; Schmidt, I.; Thamyongkit, P.; Loewe, R. S.; Syomin, D.; Diers, J. R.; Zhao, Q.; Misra, V.; Lindsey, J. S.; Bocian, D. F. Synthesis and Film-Forming Properties of Ethynylporphyrins. *Chem. Mater.* **2005**, *17*, 3728–3742.

37. Lu, Y. F.; Fan, H. Y.; Stump, A.; Ward, T. L.; Rieker, T.; Brinker, C. J. Aerosol-Assisted Self-Assembly of Mesostructured Spherical Nanoparticles. *Nature* **1999**, *398*, 223–226.

38. Moon, J. H.; Yi, G. R.; Yang, S. M.; Pine, D. J.; Bin Park, S. Electrospray-Assisted Fabrication of Uniform Photonic Balls. *Adv. Mater.* **2004**, *16*, 605–609.

39. Lee, S. Y.; Gradon, L.; Janeczko, S.; Iskandar, F.; Okuyama, K. Formation of Highly Ordered Nanostructures by Drying Micrometer Colloidal Droplets. *ACS Nano* **2010**, *4*, 4717–4724.

40. Wang, W. N.; Park, J.; Biswas, P. Rapid Synthesis of Nanostructured Cu-TiO<sub>2</sub>-SiO<sub>2</sub> Composites for CO<sub>2</sub> Photoreduction by Evaporation Driven Self-Assembly. *Catal. Sci. Technol.* **2011**, *1*, 593–600.

41. Wu, C.; Lee, D.; Zachariah, M. R. Aerosol-Based Self-Assembly of Nanoparticles into Solid or Hollow Mesospheres. *Langmuir* **2010**, *26*, 4327–4330.

42. Langley, G. J.; Hecquet, E.; Morris, I. P.; Hamilton, D. G. Direct Observation of Associative Behaviour by Electrospray Ionization: Self-Assembly - Fact or Fiction? *Rapid Commun. Mass Spectrom.* **1997**, *11*, 165–170.

43. Alcalde, E.; Mesquida, N.; Fernandez, I.; Giralt, E. Novel Charged [1<sub>4</sub>] Azolophanes: Associative Behaviour Revealed by Electrospray Ionization. *Rapid Commun. Mass Spectrom.* **2000**, *14*, 1014–1016.

44. Novoderezhkin, V.; Taisova, A.; Fetisova, Z. G. Unit Building Block of the Oligomeric Chlorosomal Antenna of the Green Photosynthetic Bacterium *Chloroflexus aurantiacus*: Modeling of Nonlinear Optical Spectra. *Chem. Phys. Lett.* **2001**, *335*, 234–240.

45. Muenter, A. A.; Brumbaugh, D. V.; Apolito, J.; Horn, L. A.; Spano, F. C.; Mukamel, S. Size Dependence of Excited-State Dynamics for J-Aggregates at Silver Bromide Interfaces. *J. Phys. Chem.* **1992**, *96*, 2783–2790.

46. Roden, J.; Strunz, W. T.; Eisfeld, A. Spectral Properties of Molecular Oligomers. A Non-Markovian Quantum State Diffusion Approach. *Int. J. Mod. Phys. B* **2010**, *24*, 5060–5067.

47. Basak, S.; Chen, D. R.; Biswas, P. Electrospray of Ionic Precursor Solutions to Synthesize Iron Oxide Nanoparticles: Modified Scaling Law. *Chem. Eng. Sci.* **2007**, *62*, 1263–1268.

48. Chen, D.-R.; Pui, D. Y. H. Experimental Investigation of Scaling Laws for Electrospraying: Dielectric Constant Effect. *Aerosol Sci. Technol.* **1997**, *27*, 367–380.

49. Kashchiev, D. *Nucleation*; Elsevier Science, 2000.

50. Chen, D. R.; Pui, D. Y. H.; Kaufman, S. L. Electrospraying of Conducting Liquids for Monodisperse Aerosol Generation in the 4 nm to 1.8  $\mu$ m Range. *J. Aerosol Sci.* **1995**, *26*, 963–978.

51. Hinds, W. C. *Aerosol Technology: Properties, Behavior, and Measurement of Airborne Particles*, 2nd ed.; John Wiley & Sons, Inc.: New York, 1999.